Promotion Effect and Mechanism of the Addition of Mo on the Enhanced Low Temperature SCR of NOx by NH3 over MnOx/γ-Al2O3 Catalysts

Gang Yang, Haitao Zhao, Xiang Luo, Kaiqi Shi, Haibao Zhao, Wenkai Wang, Quhan Chen, Hua Fan, Tao Wu

University of Nottingham
UK | CHINA | MALAYSIA

University of Nottingham Ningbo China, 199 Taikang East Road, Ningbo, 315100, China

First published 2019

University of Nottingham
UK | CHINA | MALAYSIA

Promotion Effect and Mechanism of the Addition of Mo on the Enhanced Low Temperature SCR of NO_x by NH_3 over MnO_x/γ-Al_2O_3 Catalysts

Gang Yang[a,b], Haitao Zhao[a,b], Xiang Luo[a,b], Kaiqi Shi[a,b], Haibao Zhao[d], Wenkai Wang[b], Quhan Chen[b], Hua Fan[c,*], Tao Wu[a,b,*]

a, New Materials Institute, The University of Nottingham Ningbo China, Ningbo 315100, China

b, Municipal Key Laboratory of Clean Energy Conversion Technologies, The University of Nottingham Ningbo China, Ningbo 315100, China,

c, School of Resources Environmental & Chemical Engineering, Nanchang University, Nanchang, 330031, China

d, Zhejiang Feida Environmental Science & Technology CO., LTD, Zhuji, 311899, China.

Abstract

A series of Mn/γ-Al_2O_3 and $MnMo/\gamma$-Al_2O_3 catalysts were prepared by using Incipient Wetness Impregnation (IWI) method. The catalytic performance tests showed that the $Mn_3Mo_{1.25}/\gamma$-Al_2O_3 demonstrated a higher SCR performance (NO conversion of around 96%) at a broad low temperature range (150 to 300° C). The characterization showed that the addition of Mo to the Mn/γ-Al_2O_3 catalysts could promote the dispersion of MnO_x on the surface of γ-Al_2O_3. The adsorption of NO could form two different species, nitrites and nitrates on the surface of the catalyst. The presence of nitrites is beneficial to low temperature SCR. It is also found that the existence of Mo in the catalyst favours the formation of Mn^{3+}, which plays a critical role in the adsorption of NH_3 and therefore improves NH_3 adsorption capacity of the MnO_x/γ-Al_2O_3 catalysts. The low temperature SCR of the $Mn_3Mo_{1.25}/\gamma$-Al_2O_3 catalyst was found to mainly follow L-H mechanism, but E-R mechanism also plays a role to some extent. Moreover, it is also found that the addition of Mo not only mitigates the deactivation of catalysts, but also broadens the effective temperature range of the SCR catalyst.

Keywords：Low temperature SCR; $MnMo/\gamma$-Al_2O_3; Mo addition; Promotion effects; Mechanism

1. Introduction

The emission of nitrogen oxides (NO_x) from combustion processes is associated with a series of severe environmental problems, such as acid rain and ozone depletion, has become an issue of great concern for decades [1-3]. To address this problem, the selective catalytic reduction (SCR) of NO_x by NH_3 has been applied to treat flue gas from stationary and mobile sources [4, 5]. At coal-fired power stations, V_2O_5-WO_3/TiO_2 is the most commonly used SCR catalyst. However, the high operating temperature window of 300 - 400°C is associated with a variety of problems [6, 7], such as the possible oxidation of SO_2 and the high energy consumption [8, 9]. Therefore, there is a need for the development of low temperature SCR catalysts, which has attracted a wide attention in recent years [10, 11].

The manganese-based catalyst is a good alternative to vanadium-based SCR catalysts, which has demonstrated high catalytic activity and selectivity at low temperature [9, 12-20]. Mn-based oxides catalysts, such as MnO_x-CeO_2/meso-TiO_2[21], MnO_2-(Co_3O_4)/TiO_2[22] and nano-flaky MnO_x supported on carbon nanotubes [16], have outstanding SCR activity at low temperatures. The addition of transition and/or rare earth metals, such as Fe, Ce and Sb etc, has been found to have positive effects on the performance of these Mn-based catalysts [20, 23-26]. However, their operating temperature window was narrow. The development of novel SCR catalysts, which are highly efficient at different temperature levels for different applications is highly desirable but remains very challenging [14].

Previous studies have shown that Mo can promote the distribution of active constituents on the support and subsequently enhances the activity of the catalyst [27]. Moreover, most researchers believed that low temperature SCR reaction follows Eley-Rideal (E-R) mechanism [28, 29]. However, to date, very little work has been carried out on the addition of molybdenum to manganese-based catalysts (MnMo/γ-Al_2O_3) to improve its low temperature SCR performance [30].

In this study, Mo was doped on the $Mn/\gamma\text{-}Al_2O_3$ catalysts via Incipient Wetness Impregnation (IWI) method aiming at improving its low temperature SCR performance. Systematic characterisation and testing were carried out to show the effects of Mo addition on catalytic performance of the $Mn_xMo_y/\gamma\text{-}Al_2O_3$. Moreover, the mechanism of the SCR process over the Mo-modified catalyst at low temperature was investigated.

2 Experimental

2.1 Preparation of catalysts

In this research, a series of Mn-based catalysts with different Mo and Mn loadings supported on $\gamma\text{-}Al_2O_3$ were prepared via IWI method (binary metal catalysts were prepared with a two-step IWI method)

Chemicals of AR grade, such as $Mn(NO_3)_2{\bullet}4H_2O$ and $(NH_4)_6Mo_7O_{24}{\bullet}4H_2O$, were acquired from Sinopharm Chemical Reagent Co., Ltd and used as precursors for the preparation of the catalysts. To prepare a $Mn_xMo_y/\gamma\text{-}Al_2O_3$ catalyst, a controlled amount of $(NH_4)_6Mo_7O_{24}{\bullet}4H_2O$ was loaded on $\gamma\text{-}Al_2O_3$ via IWI method, followed by drying at 120°C for 24h and calcination at 520°C for 12h. The sample prepared was then impregnated again with certain quantity of the Mn precursor, followed by drying at 120°C for 24h and calcination at 520°C for 12h. The detailed procedure for the preparation of these catalysts was described elsewhere in our previous research [31, 32].

In this study, the $Mn_x/\gamma\text{-}Al_2O_3$ catalysts means x wt% of Mn in the catalyst, while the $Mn_xMo_y/\gamma\text{-}Al_2O_3$ suggests y wt% of Mo in the catalyst.

2.2 Characterization of catalysts

The specific area of samples prepared in this study was characterised by N_2 adsorption/desorption at -196 °C using a Micromeritics ASAP 2020, the procedure of which is described elsewhere in literature [31]. The crystal phases of the catalysts were analysed by using an X-Ray Diffraction (XRD, Bruker D8 Advance) with Cu Kα radiation. Oxidation states of metal species in the catalysts were also analysed using an X-Ray Photoelectron Spectroscopy (XPS Axis Ultra DLD

Multifunctional) [33]. The C^{1s} peak at 284.8eV was used as the standard for calibration. The element compositions of catalysts were analysed by X-Ray Fluorescence (XRF, Bruker s8 TIGER). Morphology, nanostructures and elemental distribution of catalysts were examined using Transmission Electron Microscopy (TEM, FEI Tecnai G2F20). The H_2-temperature programmed reduction (H_2-TPR) was performed to investigate the redox of the samples. Ammonia (NH_3) Temperature Programmed Desorption (NH_3-TPD) method was also carried out to show the quantity and strength of acidic sites on the surface of the catalysts, which was carried out in a Micromeritics AutoChem II 2920 with a heating rate of 10°C /min and NH_3 adsorption for 30min at a flowrate of 30mL/min. NH_3 adsorptions on the surface of catalysts were carried out on a Fourier Transform Infrared Spectroscopy (FTIR, Bruker vertex 70). NO-TPD was performed in a specially designed reactor with gas composition measured by a flue gas analyser (Vario Plus, MRU, Germany).

2.3 Measurement of catalytic activity

The prepared sample was loaded into a fixed-bed reactor and exposed to a simulated flue gas containing NO_x (500 ppm), NH_3 (500 ppm), O_2 (3vol%), and N_2. The gas hourly space velocity (GHSV) adopted in this study was 3 5000·h^{-1}. Prior to each test, NO_x concentration at the inlet ($[NO_x]_{in}$) was measured to confirm the initial concentration and to minimise experimental errors. The concentration of NO_x at the outlet ($[NO_x]_{out}$) was continuously monitored by the Flue Gas Analyser (MRU Vario Plus and Testo 350, Germany). The NO_x removal efficiency is therefore determined by following equation:

$$NOx\ removal\ efficiency\ (\%) = \frac{[NOx]_{in} - [NOx]_{out}}{[NOx]_{in}} \times 100\% \quad (1)$$

3 Results and discussion

3.1. Catalytic performance

Low temperature catalytic activity of the $Mn_x/\gamma\text{-}Al_2O_3$ and $Mn_xMo_y/\gamma\text{-}Al_2O_3$ catalysts was tested in a downflow fixed-bed reactor. NO_x removal efficiency of the four catalysts is illustrated in Fig.

1(a). In Fig. 1(b), $Mn_3/\gamma\text{-}Al_2O_3$ showed outstanding low temperature NH_3-SCR activities, but the optimal operation temperature was at 250˚C. In order to further improve the low temperature NH_3-SCR activity of the $Mn_x/\gamma\text{-}Al_2O_3$ catalysts, Mo was added to modify the $Mn_x/\gamma\text{-}Al_2O_3$ catalysts. In Fig. 1(a), $\gamma\text{-}Al_2O_3$ and $Mo_y/\gamma\text{-}Al_2O_3$ did not show any SCR activity in a broad temperature range. It is obvious that the NO conversion of $Mn_3/\gamma\text{-}Al_2O_3$ was below 90% at 150°C, above 90% when temperature was raised to 200 and 250°C, but deteriorated when temperature was raised to higher levels. However, the impregnation of Mo significantly improved the low temperature catalytic performance of the $Mn_3Mo_{1.25}/\gamma\text{-}Al_2O_3$ catalyst, which showed a remarkable promoting effect at 150°C (NO conversion of 96%), and expanded the effective temperature window to 150-300°C. It was found that at higher Mo loadings, the optimal SCR temperature window started to shift to high temperature levels as shown in Fig. 1(c), which suggests that Mo is a good moderator for the adjustment of effective temperature of SCR reaction. Therefore, it can be concluded that the addition of Mo not only promotes the SCR activity of the $Mn_x/\gamma\text{-}Al_2O_3$ catalyst, but also adjusts the effective temperature range of the catalyst.

The effect of H_2O and SO_2 on the activity of $Mn_3Mo_{1.25}/\gamma\text{-}Al_2O_3$ catalysts is in Fig. 1(d). When 100ppm SO_2 and 5% H_2O were introduced into the reactant gas mixture, the NO conversion of the $Mn_3Mo_{1.25}/\gamma\text{-}Al_2O_3$ dropped to 81% after 2h, which is similar as what is reported by other researchers [34-36]. However, when the supply of SO_2 and H_2O was stopped, the NO conversion increased to about 91%. The decrease of NO conversion could be responsible for the deposit of sulphate on the catalyst surface[24]. The results indicated that the $Mn_3Mo_{1.25}/\gamma\text{-}Al_2O_3$ has resistance to SO_2 and H_2O. In Fig. 1(d), the durability of $Mn_3Mo_{1.25}/\gamma\text{-}Al_2O_3$ and $Mn_3Mo_{1.25}/\gamma\text{-}Al_2O_3$ was also conducted at 150^{o} C. The durability performance of the $Mn_3Mo_{1.25}/\gamma\text{-}Al_2O_3$ was much better than that of $Mn_3/\gamma\text{-}Al_2O_3$. NO conversion of $Mn_3Mo_{1.25}/\gamma\text{-}Al_2O_3$ decreased slightly to 95% after 20h, which indicated that Mo enhanced the durability of $Mn_x/\gamma\text{-}Al_2O_3$ catalysts.

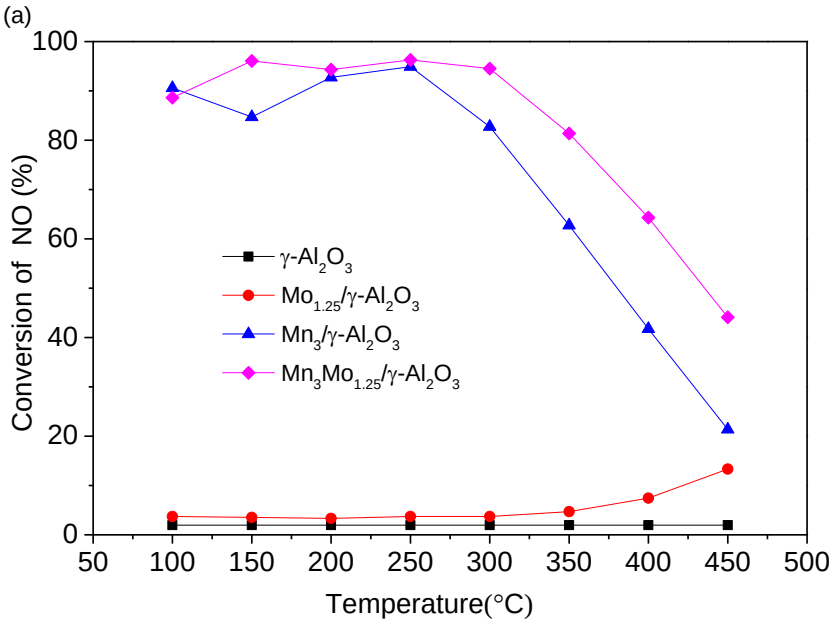
(a)
Conversion of NO (%)
Temperature(°C)
γ-Al2O3
Mo1.25/γ-Al2O3
Mn3/γ-Al2O3
Mn3Mo1.25/γ-Al2O3

125

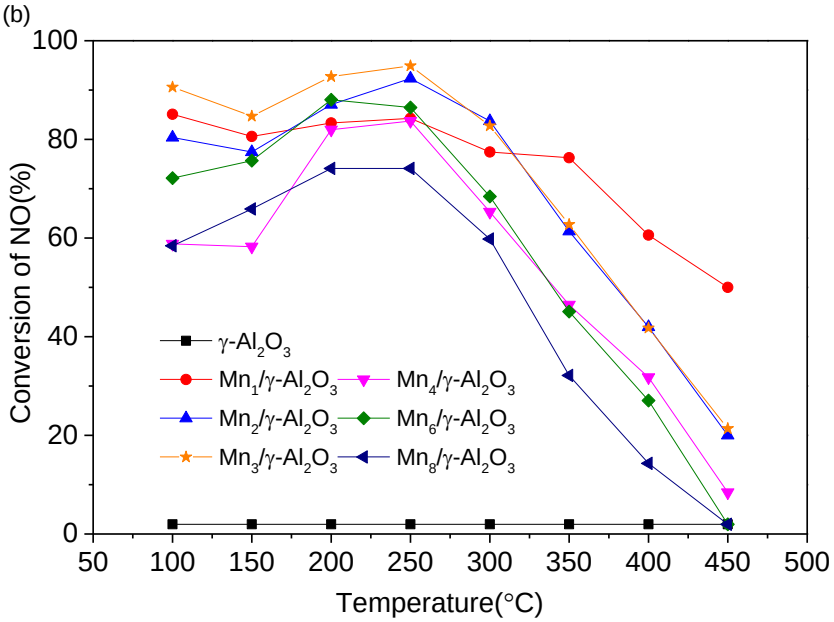
(b)
Conversion of NO(%)
Temperature(°C)
γ-Al2O3
Mn1/γ-Al2O3
Mn4/γ-Al2O3
Mn2/γ-Al2O3
Mn6/γ-Al2O3
Mn3/γ-Al2O3
Mn8/γ-Al2O3

126

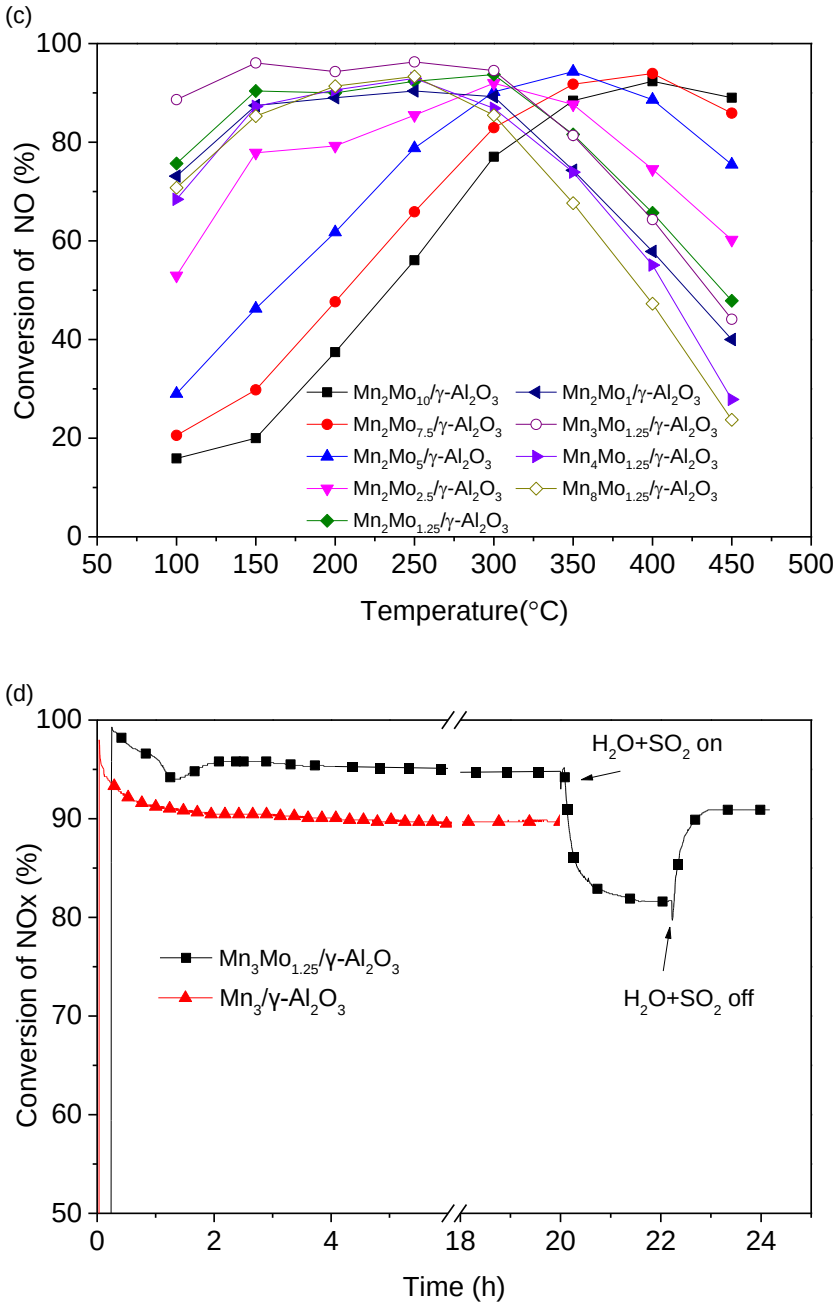

Fig.1 NO conversion over different catalysts under different gas atmosphere. Reaction condition: (a), (b), (c), (d), [NH_3] = [NO] = 500ppm, O_2=3%, N_2 balance, GHSV=35 000h^{-1}. (d), SO_2=100ppm, H_2O=5%, Temperature 150° C.

3.2. Characterization of the catalysts

3.2.1. Effects of Mo addition on Mn dispersion

Structural and morphological properties of the catalysts were investigated by BET and XRD analyses. As shown in Table. 1, the specific surface area of the $Mn_3Mo_{1.25}/\gamma$-Al_2O_3 catalyst is larger than that of the Mn_3/γ-Al_2O_3 catalyst, which provides more active sites for low temperature NH_3-SCR reaction. In comparison with pure γ-Al_2O_3, the surface area of the γ-Al_2O_3 loaded with Mo

decreased slightly. When the Mo loading was below 5 wt %, the surface area of catalysts increased with the increase in Mo loading, which means that the addition of Mo contributes to the dispersion of active component on the support. However, further increase in Mo loading content prevents this trend. It is clear from Table 1 that when Mo loading was greater than 5 wt %, surface areas of the catalysts decreased with the increase in Mo loading. The low temperature SCR activity dropped with the increase in Mo loading. Therefore, 1.25 wt % of Mo loading was found to be the optimal that not only enhanced the dispersion of Mn on the surface of the catalysts, but also promoted the surface area to certain extent.

147 **Table.1 The surface properties of the catalysts**

Catalyst	BET surface area(m^2/g)	Pore volume(cm^3/g)	Pore size(Å)
γ-Al_2O_3	242.2	0.48	79. 7
Mn_2/γ-Al_2O_3	190.02	0.47	99.36
Mn_3/γ-Al_2O_3	216.4	0.45	82.7
Mn_4/γ-Al_2O_3	164.90	0.46	112.33
Mn_6/γ-Al_2O_3	172.18	0.40	88.08
Mn_2Mo_1/γ-Al_2O_3	194.45	0.44	90.86
$Mn_2Mo_{1.25}$/γ-Al_2O_3	207.61	0.46	89.08
$Mn_2Mo_{2.5}$/γ-Al_2O_3	209.65	0.45	86.38
Mn_2Mo_5/γ-Al_2O_3	209.91	0.42	81.16
$Mn_2Mo_{7.5}$/γ-Al_2O_3	209.53	0.42	80.42
Mn_2Mo_{10}/γ-Al_2O_3	189.67	0.37	78.93
$Mn_3Mo_{1.25}$/γ-Al_2O_3	225.7	0.46	80.7
$Mn_4Mo_{1.25}$/γ-Al_2O_3	219.70	0.45	88.11
$Mn_6Mo_{1.25}$/γ-Al_2O_3	192.38	0.41	85.81
Mo_1/γ-Al_2O_3	221.93	0.48	86.69
$Mo_{1.25}$/γ-Al_2O_3	221.18	0.52	94.70
$Mo_{2.5}$/γ-Al_2O_3	223.33	0.46	82.94
Mo_5/γ-Al_2O_3	227.67	0.45	78.85
$Mo_{7.5}$/γ-Al_2O_3	220.37	0.41	75.49
Mo_{10}/γ-Al_2O_3	211.06	0.40	75.00

148 XRD spectrum of the $Mn_3Mo_{1.25}$/γ-Al_2O_3, Mn_3/γ-Al_2O_3, $Mo_{1.25}$/γ-Al_2O_3 and γ-Al_2O_3 are shown in
149 Fig 2 (a). It is clear that the XRD patterns showed four different compounds: γ-Al_2O_3 (JCPDS 04-
150 0880), β-MnO_2 (JCPDS 24-0735), α-Mn_2O_3 (JCPDS 24-0508), while the MoO_x did not exist,
151 which was due to its low content. Pijun Gong's et al. [37] claimed that β-MnO_2 has the worst SCR
152 activity in among different MnO_2 species, while α-Mn_2O_3 was found to demonstrate high SCR
153 activity and selectivity by many researchers[38, 39]. Except for γ-Al_2O_3, the intensity of diffraction
154 peaks of Mn compounds was weak. However, in Fig 2(b), when Mn loading varied from 0 to 6
155 wt%, the diffraction peaks of α-Mn_2O_3, MnO, β-MnO_2, especially that of α-Mn_2O_3, started to

appear when Mn loading raised to 3 wt%, and the peaks intensity became higher with the increase in Mn loadings, which means bulk MnO_x species began to form and accumulated on the surface of the catalyst. However, bulk MnO_x species occupied great amount of surface space but performed poor low temperature SCR activity[40]. While doping Mo first on the support, the intensity of diffraction peaks intensity of Mn species decreased, as shown in Fig 2 (a) and (b). It can be concluded that Mo species could improve the dispersion of MnOx species on the support surface, prevent the formation of large MnO_x bulks, and strengthen the interaction between MnO_x and the support.

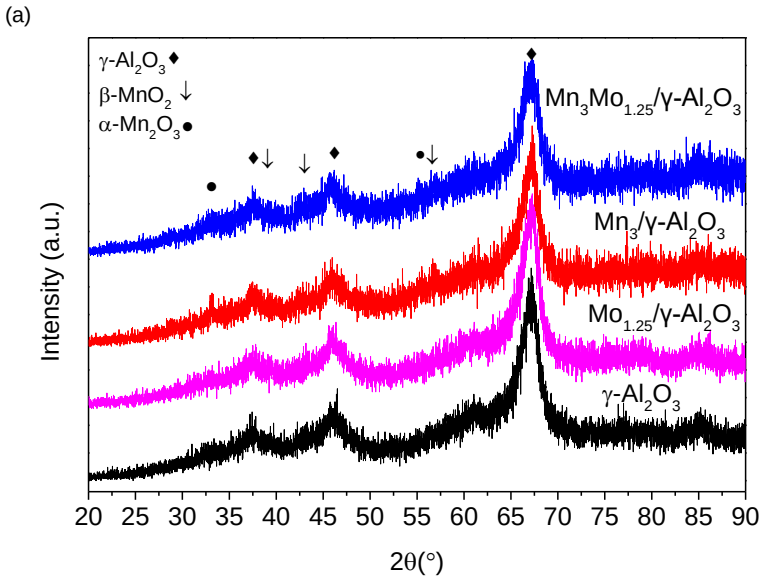

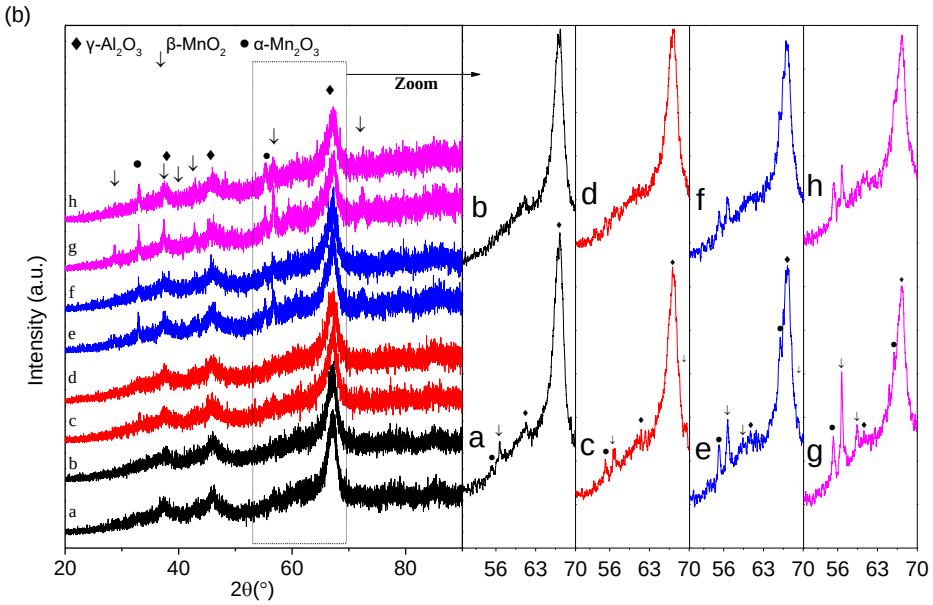

Fig.2 XRD patterns of catalysts. a. $Mn_2/\gamma\text{-}Al_2O_3$, b. $Mn_2Mo_{1.25}/\gamma\text{-}Al_2O_3$, c. $Mn_3/\gamma\text{-}Al_2O_3$, d. $Mn_3Mo_{1.25}/\gamma\text{-}Al_2O_3$, e. $Mn_4/\gamma\text{-}Al_2O_3$, f. $Mn_4Mo_{1.25}/\gamma\text{-}Al_2O_3$, g. $Mn_6/\gamma\text{-}Al_2O_3$, h. $Mn_6Mo_{1.25}/\gamma\text{-}Al_2O_3$

3.2.2. XPS, XRF and TEM-EDX

The XPS of Mn 2p (a), Mo 3d (b) are shown in Fig. 3. Different MnO_x species have specific and unique spectrums. In Fig. 3(a), $Mn3p_{3/2}$ peaks consist of three MnO_x species, Mn^{4+} (641.5-641.7eV), Mn^{3+} (541.5-541.7eV) and satellite[41]. The area ratio, respectively, represent the relative amount of species on the surface. A significant decrease in area ratio of Mn^{4+}/Mn^{3+} from 1.26 to 1.08 was observed as a result of Mo addition, which is consistent with the results of XRD analysis. It can be seen from Table 2 that the $Mn_3Mo_{1.25}/\gamma\text{-}Al_2O_3$ catalyst had a lower Mn/Al atomic ratio. Moreover, XRF and TEM/EDX tests were carried out to show the existence of different species in the catalysts. In Table 3, the mass percentage of Mn, Mo, Al and O is consistent with these species during the preparation of catalysts. Thus, it can be concluded that the Mn was well loaded on the support. In Fig. 4(a) and (b), $Mn_3Mo_{1.25}/\gamma\text{-}Al_2O_3$ is of a more uniform morphology and structure as compared with $Mn_3/\gamma\text{-}Al_2O_3$. No aggradation of MnO_x was formed on the surface of $Mo_3Mo_{1.25}/\gamma\text{-}Al_2O_3$, which means MnOx species have a better dispersion on the surface of $Mo_3Mo_{1.25}/\gamma\text{-}Al_2O_3$. The surface Mn content had a significant increase after the doping Mo, as shown in Fig. 4(c) and (d). It implied that the addition of Mo strengthens the interactions between MnO_x species and the $\gamma\text{-}Al_2O_3$, promotes the dispersion of MnO_x on the surface of support. In Fig. 3(b), it can be seen that Mo was loaded on the catalysts surface in the form of MoO_3, which was proved by Mo 3d XPS peak at 232.6 eV. In addition, it is speculated that Mo might just act as an accelerant responsible for the formation of active components, itself state does not alter on the surface of the support.

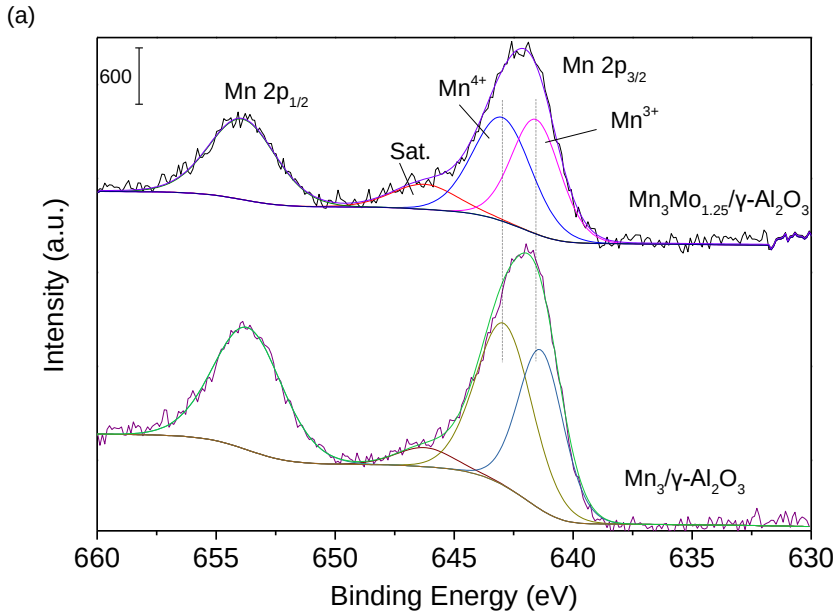

189

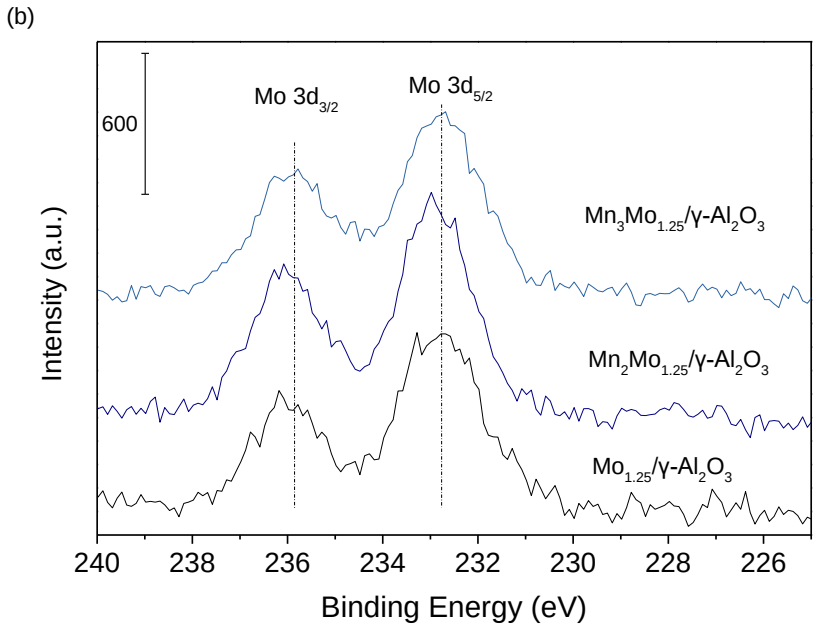

190

191 **Fig.3 XPS spectra of MnO_x/γ-Al_2O_3 catalysts before and after Mo addition**

192 **Table.2. Binding energy values and surface atomic ratio between Mn 2p for $MnO_x/\ \gamma$-Al_2O_3**
193 **catalysts before and after modified by Mo addition**

Catalyst		Binding Energy(eV)	PWHH	Mn^{4+}/Mn^{3+}	Mn/Al atomic ratio (PP)	Mo/Al atomic ratio (PP)
		Mn $2p_{3/2}$				
$Mn_3Mo_{1.25}/\gamma$-Al_2O_3	Mn^{4+}	642.97	2.8	1.08	0.046	0.018
	Mn^{3+}	641.56	2.4			
Mn_3/γ-Al_2O_3	Mn^{4+}	642.84	2.7	1.26	0.062	0
	Mn^{3+}	641.46	2.0			

194 **Table.3. The composition (wt.%) of catalysts measured by X-ray fluorescence (XRF)**

Catalyst	Mn	Mo	Al	Mn/Al atomic ratio	Mo/Al atomic ratio
$Mn_3Mo_{1.25}/\gamma\text{-}Al_2O_3$	3.17	1.33	49.7	0.0313	0.0075
$Mn_3/\gamma\text{-}Al_2O_3$	3.2	0	50.7	0.0310	0

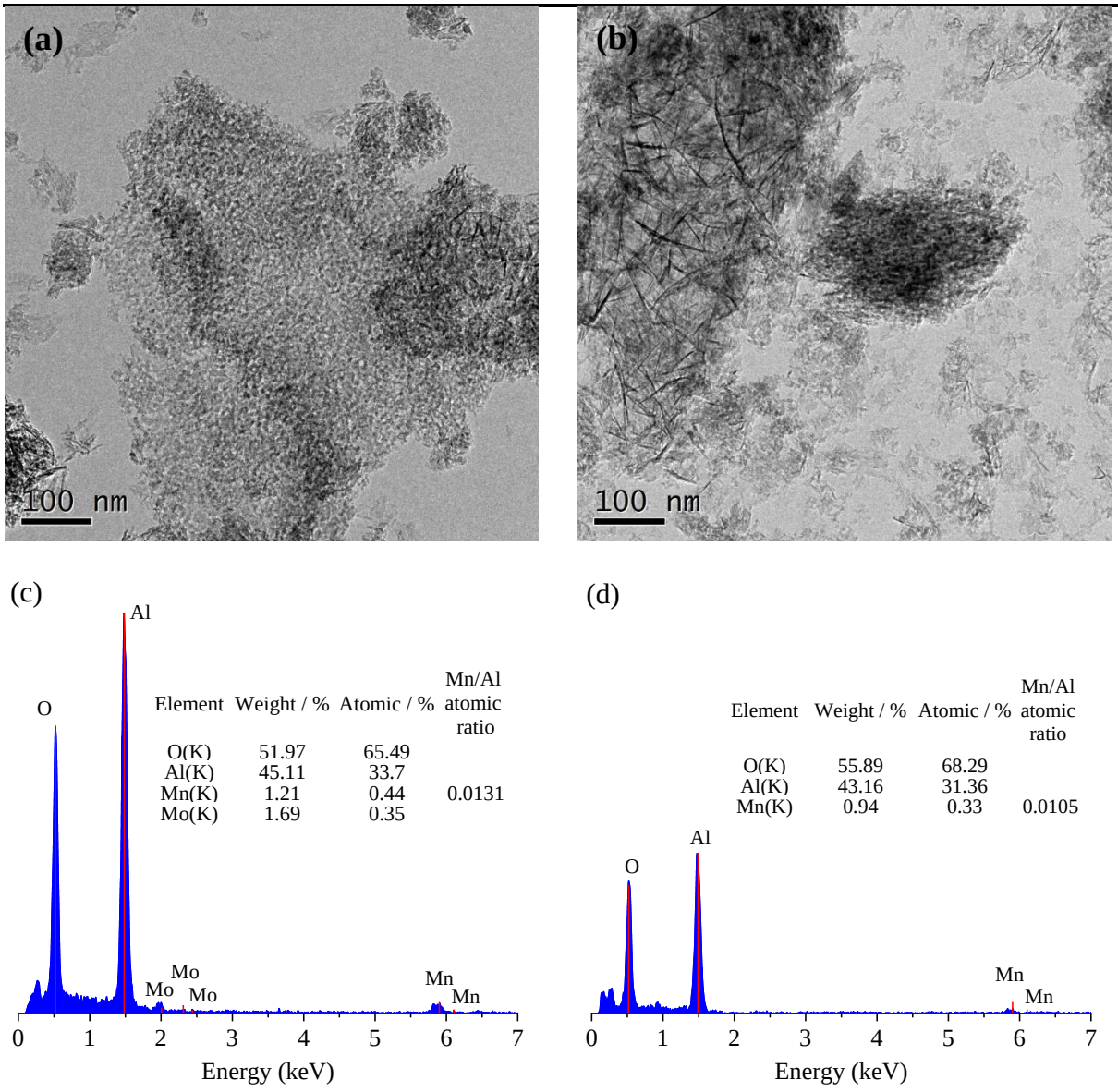

Fig.4. TEM micrographs(a and b) and EDX (c and d) spectra of $Mn_3/\gamma\text{-}Al_2O_3$ (b and d) and $Mn_3Mo_{1.25}/\gamma\text{-}Al_2O_3$ (a and c)

3.2.3. H_2-TPR

The H_2-TPR results of the $\gamma\text{-}Al_2O_3$, $Mo_{1.25}/\gamma\text{-}Al_2O_3$, $Mn_3/\gamma\text{-}Al_2O_3$, $Mn_3Mo_{1.25}/\gamma\text{-}Al_2O_3$ are shown in Fig. 5. There are four distinct reduction peaks, τ1, τ2, τ3, τ4, which are corresponding to the reduction of MnO_2 to Mn_2O_3, Mn_2O_3 to Mn_3O_4, Mn_3O_4 to MnO and MoO_3 to MoO_2

respectively[42]. Additionally, the curve of γ-Al_2O_3 did not change significantly except a noticeable drift at the high temperatures.

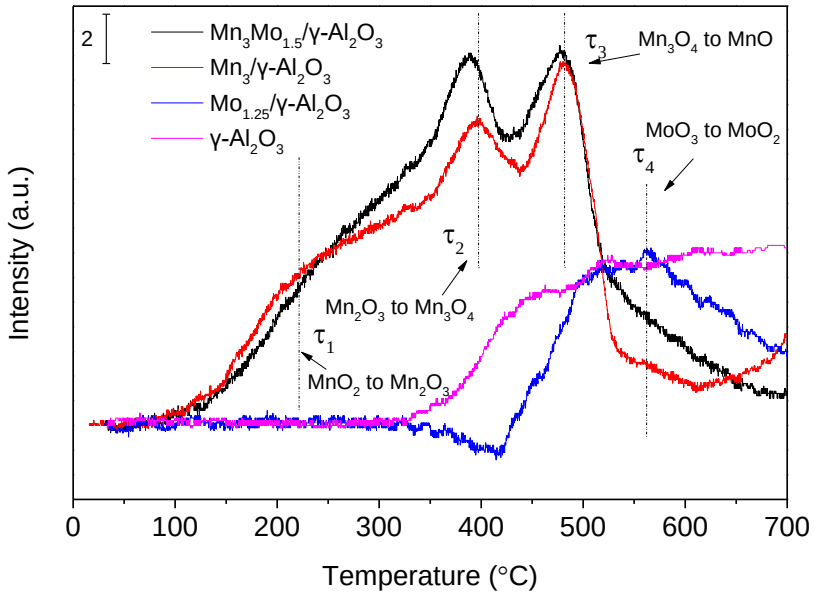

Fig.5 H_2-TPR profiles over Mo modified MnO_x/γ-Al_2O_3 catalysts

Comparing $Mn_3Mo_{1.25}$/γ-Al_2O_3 with Mn_3/γ-Al_2O_3, the temperature of τ2, τ3 decreased, which suggests that Mn_2O_3 has a stronger interaction with the support in $Mn_3Mo_{1.25}$/γ-Al_2O_3. The intensity of τ2 and τ3 also increased. Based on observations, it is speculated that the Mo in catalysts promotes the formation of Mn_2O_3, which is consistent with the results of XRD and XPS analyses. Normally, only the NH_3 being adsorbed on the Lewis acid site of Mn^{3+} shows low temperature SCR activity and can activate the ammonia to -NH_2 [5]. The -NH_2 takes part in the SCR reaction which suggests that the more Mn_2O_3 the catalyst has, the more Mn^{3+} Lewis acid sites are formed, which subsequently promotes low temperature SCR, while the MnO_2 plays a less important role in the low temperature SCR reaction. In contrast, Mn_2O_3 dominated the selective catalytic reduction performance at low temperature, which agreed well with the theory proposed by De Fang[43]. Therefore, it could be concluded that the addition of Mo could promote low temperature SCR activity of the Mn/ γ-Al_2O_3 catalyst by enabling the formation of more Lewis acid sites.

3.2.4. NH_3-TPD and FTIR

The amount and strength of surface acid sites of Mn_3/γ -Al_2O_3 catalyst before and after Mo addition was investigated using NH_3-TPD, which is shown in Fig. 6. There are three distinct peaks, which could be divided into weak, medium and strong acid sites, respectively. The temperature range of τ1, τ2 and τ3 is 150-250°C, 250-400°C and 400-500°C respectively. The $Mn_3Mo_{1.25}/\gamma$-Al_2O_3 had higher intensity at all peaks, which suggests more medium and strong acid sites existed.

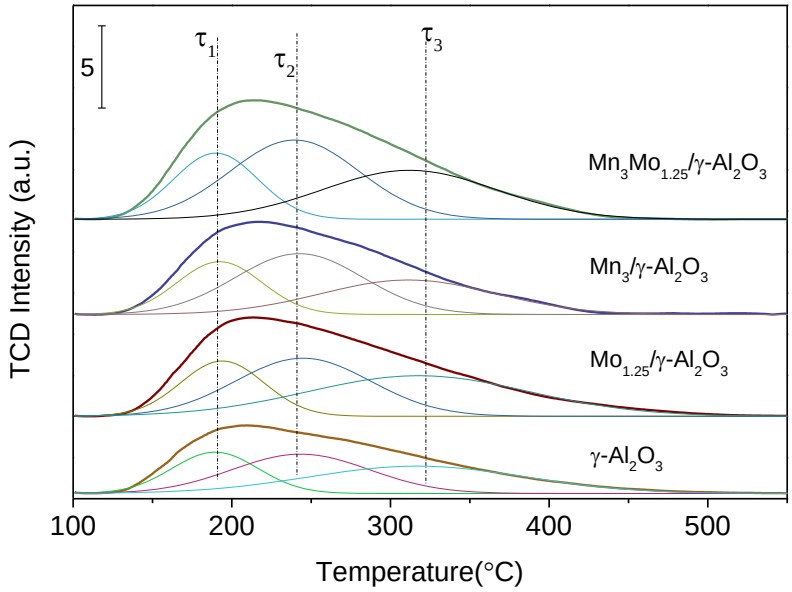

Fig.6. NH_3-TPD profiles of Mn_3/γ-Al_2O_3 catalysts before and after modified by Mo addition

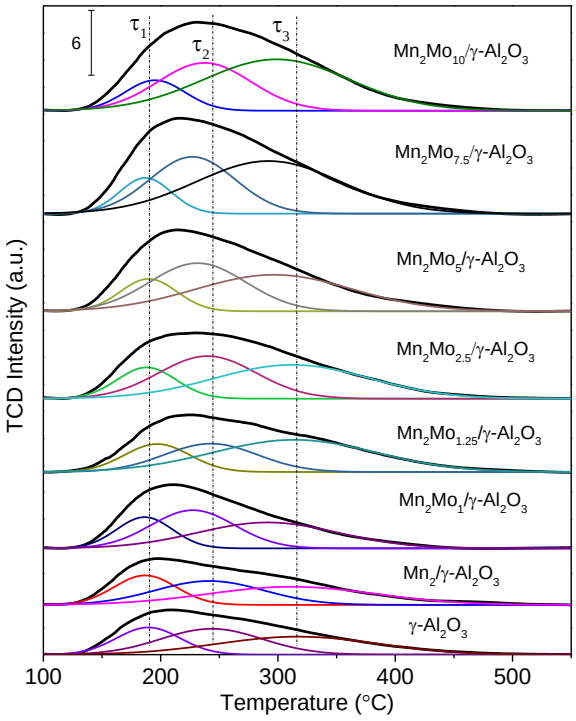

Fig. 7. NH_3-TPD profiles over Mn_2/γ-Al_2O_3 catalysts with different Mo loadings

Moreover, catalytic activity of the $Mn_x/\gamma\text{-}Al_2O_3$ with different Mo loadings was investigated as shown in Fig. 7. The strong and medium acid sites of catalyst increased significantly with the increase in Mo loadings. It is also found that a higher Mo loading led to a higher catalytic temperature of the catalysts in Fig. 1(c). Therefore, the low Mo content (1.25 wt%) favoured the low temperature SCR.

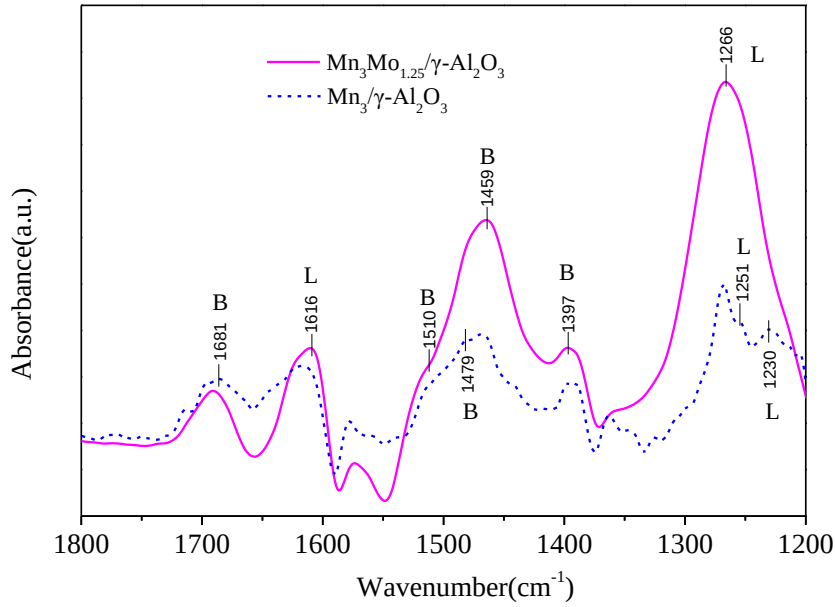

Fig. 8. FTIR spectra of $Mn_3/\gamma\text{-}Al_2O_3$ and $Mn_3Mo_{1.25}/\gamma\text{-}Al_2O_3$ treated in flowing 500ppm NH_3 at 100°C until saturation and then purged by N_2.

Fig. 8 shows the FTIR spectra of NH_3 adsorption over $Mn_3/\gamma\text{-}Al_2O_3$ and $Mn_3Mo_{1.25}/\gamma\text{-}Al_2O_3$ catalysts at 100°C. For $Mn_3Mo_{1.25}/\gamma\text{-}Al_2O_3$, two strong bands at 1266 and 1465 cm^{-1} and two relatively weaker bands at 1616 and 1681 cm^{-1} were observed. The bands at 1230, 1251, 1266, 1616 cm^{-1} can be assigned to bending vibrations of N-H bonds in the NH_3 linked to Lewis acidic sites[44]. The bands at 1397cm^{-1} were almost same, resulted from over NH_3 adsorption on $\gamma\text{-}Al_2O_3$[45]. The bands at 1459 and 1479cm^{-1} were observed due to NH_3 adsorbed on Brönsted acidic sites. What's more, an amide($-NH_2$) species also was observed at 1510cm^{-1}. The bands at 1616cm^{-1} (assigned to Lewis acidic sites) and 1681cm^{-1} (assigned to Brönsted acidic sites mainly) are mainly came from NH_3 adsorption on $\gamma\text{-}Al_2O_3$. In previous report[46], molybdenyl species

were unsaturated on the catalyst surface and were deranged easily by adsorption of ammonia. In Fig. 8, it can be seen that Lewis and Brönsted acidic sites at 1266 and 1465 cm^{-1} were significantly enhanced after the modification of Mo. This confirms what was found in NH3-TPD analysis.

3.2.5. NO-TPD

Fig. 9 shows the NO-TPD profiles of the $Mn_3/\gamma\text{-}Al_2O_3$ catalyst before and after Mo addition. Two desorption peaks can be observed in Fig. 9, which contained a broad peak in the low temperature region (LT-peak) and a strong peak at higher temperature region (HT-peak). The nitroso species formed from the adsorbed NO at LT-peak will react with ammonia [45]. In contrast, the nitro compounds formed from the NO adsorbed at HT-peak only decomposed at high temperature and reacted with $–NH_2$[47]. Therefore, the area ratio between LT-peak and HT-peak could be utilized to evaluate the activity of SCR catalyst and investigate the mechanism of catalytic process. In Fig. 9, after the addition of Mo, there is a shift in LT-peak and HT-peak toward lower temperature region and the height of peak decreased, which indicates that the $Mn_3Mo_{1.25}/\gamma\text{-}Al_2O_3$ had a lower SCR activity temperature. In addition, the area ratio between LT-peak and HT-peak increased from 4.6 to 5.13, which means that more nitroso species formed on the $Mn_3Mo_{1.25}/\gamma\text{-}Al_2O_3$ so that higher low temperature SCR activity.

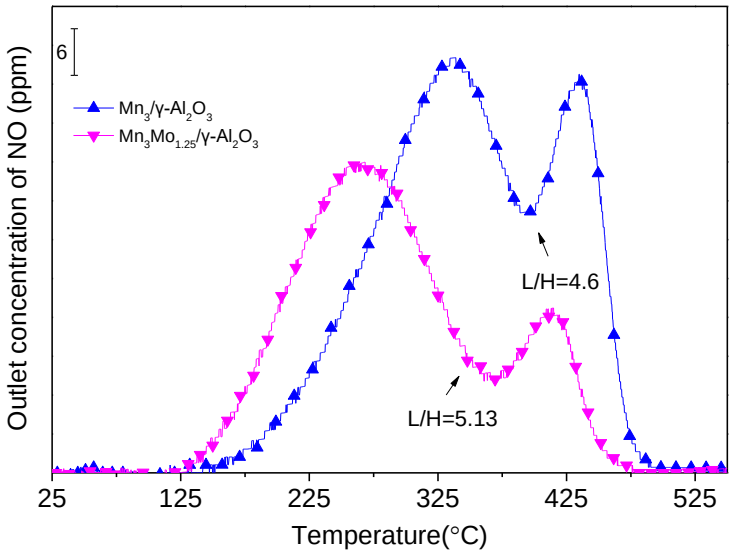

Fig. 9. NO-TPD profiles of the $Mn_3/\gamma\text{-}Al_2O_3$ and $Mn_3Mo_{1.25}/\gamma\text{-}Al_2O_3$

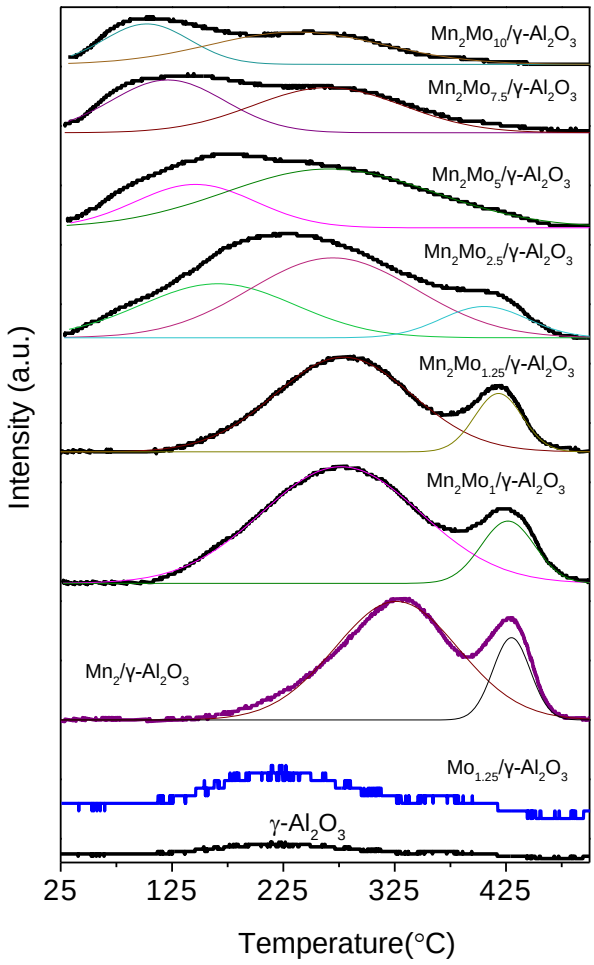

Fig. 10. NO-TPD profiles of the Mn_2Mo_x/γ-Al_2O_3

Fig. 10 shows that the LT-peak of Mn catalyst shifted to lower temperature region with the Mo loading increased to 2.5 wt% and a new desorption peak formed below 200˚C. With the increase in Mo loading to 10 wt%, the center of the new peak shifted to below 100˚C. Meanwhile, the intensity of HT-peaks weakened gradually and disappeared when the Mo loading was 7.5 wt%. This suggests that the addition of Mo had a significant influence on the adsorption of NO.

3.2.6. Mechanism of low temperature SCR over Mo-modified Mn-based catalyst

Four sets of NO adsorption and desorption experiment were carried out to investigate the adsorption of NH_3 and NO on the $Mn_3Mo_{1.25}/\gamma$ -Al_2O_3 catalysts.

I: The adsorption of NH_3 (500ppm) +NO (500ppm) +O_2 (3%) at 25°C for 1h, and then purged with N_2 until outlet concentration of NO became below 5ppm, followed by performing TPD process at 10°C/min;

II: The adsorption of NH_3 (500ppm) + O_2 (3%) at 25°C for 1h, switched to the adsorption of NO (500ppm) + O_2 (3%) at 25°C for 1h, and then purged with N_2 until outlet concentration of NO became below 5ppm, followed by performing TPD process at 10°C /min;

III: The adsorption of NO (500ppm) +O_2 (3%) at 25°C for 1h, switched to the adsorption of NH_3 (500ppm) + O_2 (3%) at 25°C for 1h, and then purged with N_2 until outlet concentration of NO became below 5ppm, followed by performing TPD Process at 10°C /min;

IV: The adsorption of NO (500ppm) +O_2 (3%) at 25°C for 1h, and then purged with N_2 until outlet concentration of NO became below 5ppm, followed by performing TPD Process at 10°C /min.

In Fig. 11, Curve III coincided with Curve IV resulted from the adsorption of NO on the fresh catalyst. However, Curve I shifted as compared with Curves III and IV when NH_3 and NO were simultaneously introduced, which indicates that NH_3 adsorbs on certain sites competitively with NO. Curve II shifted up significantly in the first 25 min, and then shifted down to the level of curve III and IV. It can therefore be concluded that some of the adsorption sites are occupied randomly by NH_3 owing to NH_3 preferentially adsorbed on the catalyst. According to the calculation, the adsorption capacity of Curve I was larger than that of Curve II, which is attributed to gas phase NH_3 being competitively adsorbed with NO on the catalyst surface. Therefore, the adsorption sites of the catalysts could be classified into four types: Type 1, adsorbs NH_3 preferentially; Type 2, adsorbs NO preferentially; Type 3, adsorbs NH_3 competitively, and Type 4, random adsorption sites, on which both NH_3 and NO can be adsorbed depending on their molecular movement.

As shown in Fig. 12, TPD Curves i and ii did not show high temperature desorption peak of NO and NO_2. TPD Curves iii and iv are similar, but low temperature desorption peaks of curve iii for NO are weak and high temperature desorption peaks also shifted. Compared Curve i with iii, TPD results did not show high temperature desorption peaks, which indicated that bidentate nitrate and bridge nitrate were not easy to form on the surface treated by NH_3[5]. It is speculated that O_2 will

accelerate the formation of these stable NO complexes, which only react with NH_3 at high temperature and are responsible for the deactivation of SCR catalysts.

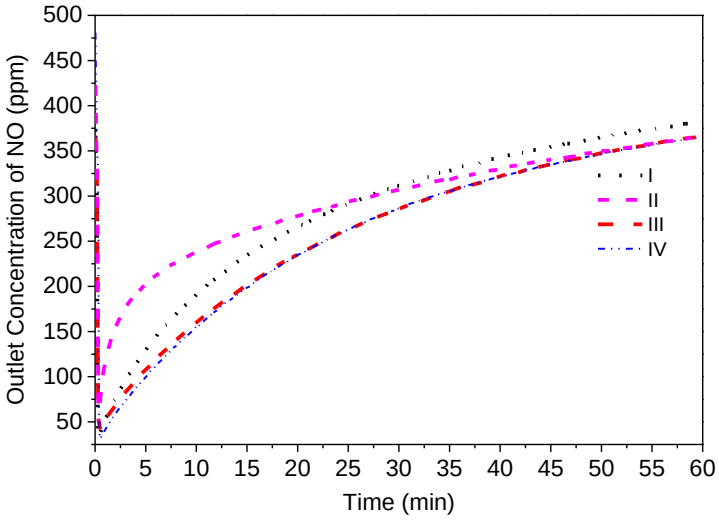

Fig. 11 NO adsorption over the $Mn_3Mo_{1.25}/\gamma\text{-}Al_2O_3$ catalyst

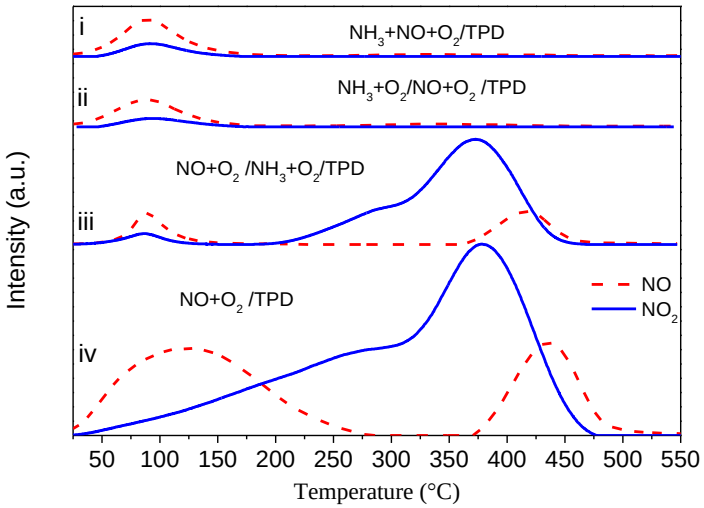

Fig. 12 TPD profiles of the NO adsorption over the $Mn_3Mo_{1.25}/\gamma\text{-}Al_2O_3$ catalyst

It is generally believed that SCR reaction starts with the adsorption of NH_3. But the mechanisms of low temperature SCR for catalysts with different active components and support are different. Marban et al. [48] suggested that there are two different SCR mechanisms associated with different NH_3 species. In Fig. 12, NO-TPD peaks disappeared in Curves i and ii, which is attributed to the reaction between NO and ad-NH_3 on the catalyst surface. As shown in Fig. 13, the $Mn_3Mo_{1.25}/\gamma\text{-}Al_2O_3$ catalyst adsorbed NO for 1h and then carried out TPD test from 25˚C to 150˚C (Process I), followed by purging with N_2 for 1h (Process II). In Process III, NH_3 and O_2 were introduced, and temperature was kept at 150˚C. In Process IV, TPD test was carried out from 150˚C to 630˚C. In

order to compare, a similar test without Process III was taken into consideration, which is also shown in Fig. 13 (dashed line). The amount of NO_x being adsorbed at low temperature around 250˚C decreased, even disappeared, and high temperature species were also reduced to some extent, which directly proves that low temperature SCR proceeds between the adsorbed NH_3 species and the adsorbed NO species via Langmuir-Hinshelwood (L-H) mechanism.

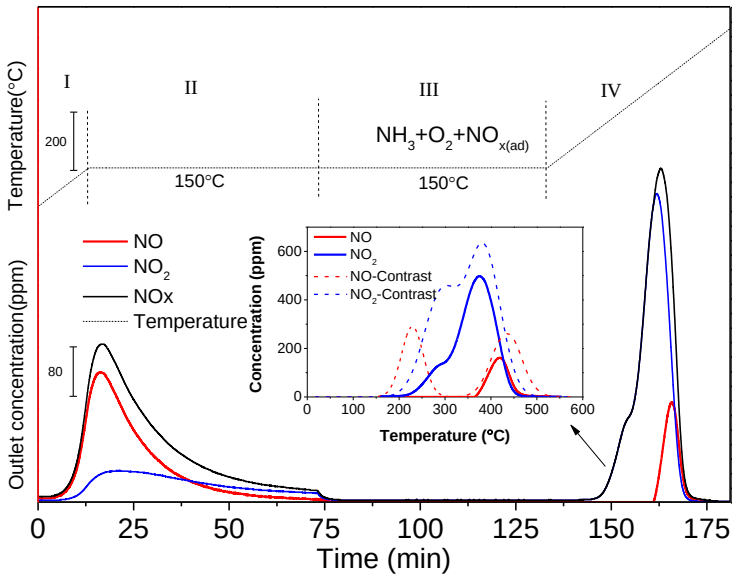

Fig. 13 TPD profiles of NO adsorption over the $Mn_3Mo_{1.25}/\gamma$-Al_2O_3 catalyst, Process I: TPD from 25-150°C; Process II: N_2 purging for 60min; Process III: adsorbed NO reacted with NH_3; Process IV: TPD from 150°C-630°C

In this study, the addition of Mo was found to improve NH_3 adsorption capacity of the catalyst. With the increase in Mo loadings, the amount of surface acid sites increased, which was vital to SCR reaction. In Fig. 14, when in the presence of gas phase O_2, the adsorption peaks of NO and NO_2 decreased. Therefore, it can be concluded that the addition of Mo could reduce NO adsorption on the catalysts surface but did not result in a lower low temperature SCR activity. Instead, the low temperature SCR efficiency of the $Mn_3Mo_{1.25}/\gamma$-Al_2O_3 was much higher than that of the Mn_3/γ-Al_2O_3 catalyst. Additionally, in Fig.12, Curve II showed a small desorption peak at 100° C as compared with Curve III. This means that the NOx being desorbed reacted with the NH_3 that is adsorbed on the catalyst when the temperature was raised. Therefore, it is illustrated that low temperature SCR reaction could proceed via Eley-Rideal (E-R) path.

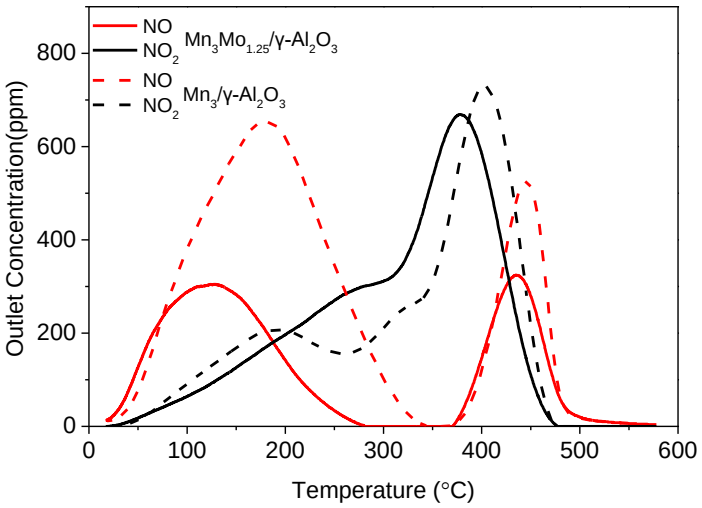

335

336 **Fig. 14 Effect of O_2 on the NO adsorption over the $Mn_3/\gamma\text{-}Al_2O_3$ and $Mn_3Mo_{1.25}/\gamma\text{-}Al_2O_3$**
337 **catalyst**

338 It is clear that the $Mn_3Mo_{1.25}/\gamma\text{-}Al_2O_3$ catalyst performed outstanding low temperature SCR activity
339 as a result of Mo addition. It can be concluded that the addition of Mo improves the properties of
340 the catalysts in several aspects. Firstly, the addition of Mo species to the catalyst inhibits the
341 growth of MnO_x clusters, therefore leads to the good dispersion of MnO_x on the $\gamma\text{-}Al_2O_3$ surface.
342 Secondly, the addition of Mo enhances the formation of Mn_2O_3 on the catalyst, which accelerates
343 the formation of intermediates, whereafter the $-NH_3$ is transformed into $-NH_2$ via H-abstraction.
344 Thirdly, the addition of Mo on the catalysts mitigates the deactivation of the catalysts. In Fig. 13,
345 NO adsorbed species at HT-Peak region were very difficult to react with NH_3 at 150˚C. The reason
346 is that these NO formed some complexes (bridged and bidentate nitrates) that are thermally stable.
347 However, the addition of Mo could inhibit the transformation of nitrites into nitrates thus slow
348 down the self-deactivation of the catalysts.

349 Therefore, the low temperature SCR reaction is composed of 4 steps as shown in Fig. 15: Step 1,
350 the adsorption of NH_3 and NO on the surface of the catalysts; Step 2, the H-abstraction of adsorbed
351 NH_3, resulting in the formation of $-NH_2$ species as well as the formation of reactive nitrites from
352 the adsorbed NO species; Step3, the $-NH_2$ species reacted with nitrites or gas phase NO via L-H
353 and E-R mechanism, forming intermediate products $-NH_2NO$, and Step4, $-NH_2NO$ decomposed
354 into N_2 and H_2O.

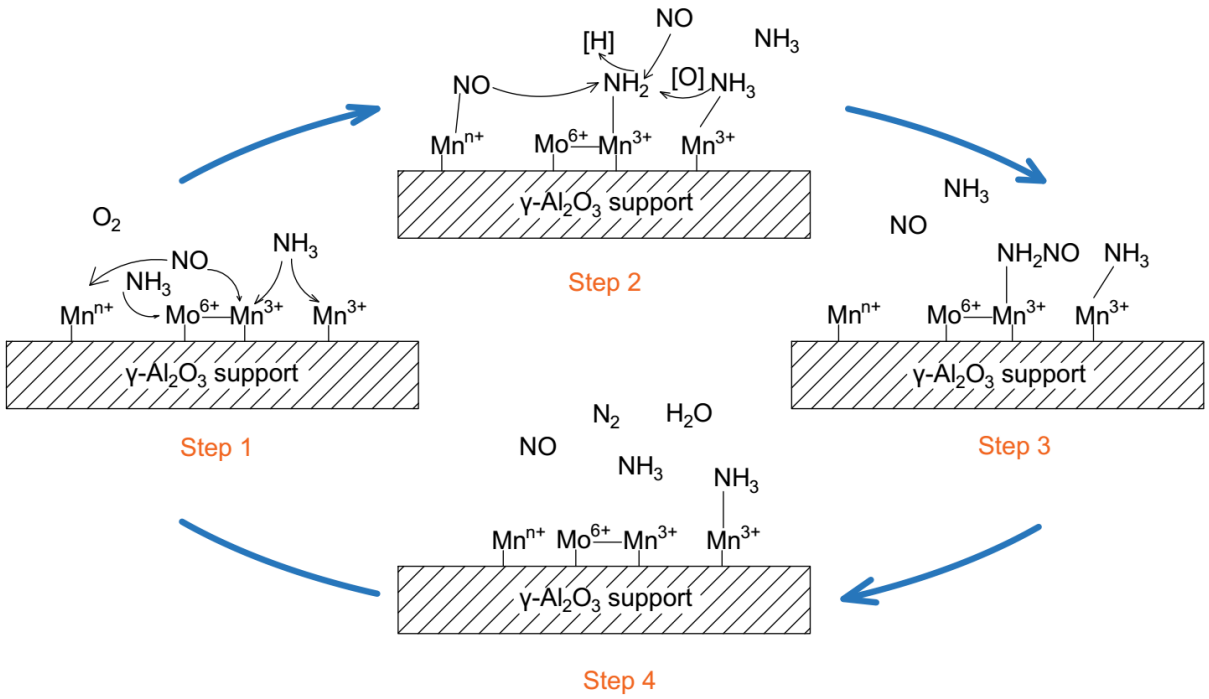

Fig. 15 Low temperature SCR reaction mechanism model

4. Conclusions

In this study, the $Mn_3Mo_{1.25}/\gamma\text{-}Al_2O_3$ catalyst achieved a high NO conversion of around 96% at 150 -300°C. It is found that the addition of Mo to Mn-based SCR catalyst could not only inhibit the growth of MnO_x bulks, favour the formation of Mn^{3+} state and promote the NH_3 adsorption capacity of the catalyst, but also act as a moderator to adjust the effective operating temperature window of the SCR reaction, which could be achieved by adjusting Mo loading. Moreover, the addition of Mo was found to mitigate the deactivation of the catalysts. The study on SCR mechanism showed that the low temperature SCR starts from the adsorption of NH_3 on Mn^{3+} sites. The low temperature SCR followed mainly E-R mechanism, but L-H mechanism also plays a role to some extent.

Acknowledgements

National Key R&D Program of China(2017YFB0603202) is acknowledged for partially sponsored this research. Authors 1 and 2 contributed equally to this work.

Reference

[1] F. Cao, J. Xiang, S. Su, P. Wang, S. Hu, L. Sun, Ag modified Mn–Ce/γ-Al_2O_3 catalyst for selective catalytic reduction of NO with NH_3 at low-temperature, Fuel Processing Technology, 135 (2015) 66-72.

[2] G. Busca, L. Lietti, G. Ramis, F. Berti, Chemical and mechanistic aspects of the selective catalytic reduction of NOx by ammonia over oxide catalysts: A review, Applied Catalysis B: Environmental, 18 (1998) 1-36.

[3] L. Sun, Q. Cao, B. Hu, J. Li, J. Hao, G. Jing, X. Tang, Synthesis, characterization and catalytic activities of vanadium–cryptomelane manganese oxides in low-temperature NO reduction with NH_3, Applied Catalysis A: General, 393 (2011) 323-330.

[4] J.A. Dumesic, N.Y. Topsøe, H. Topsøe, Y. Chen, T. Slabiak, Kinetics of Selective Catalytic Reduction of Nitric Oxide by Ammonia over Vanadia/Titania, Journal of Catalysis, 163 (1996) 409-417.

[5] W.S. Kijlstra, D.S. Brands, E.K. Poels, A. Bliek, Mechanism of the Selective Catalytic Reduction of NO with NH3 over MnOx/Al2O3 I. Adsorption and Desorption of the Single Reaction Components, Journal of Catalysis, 71 (1997) 208-218.

[6] S. Niksa, A. Freeman Sibley, Predicting the Multipollutant Performance of Utility SCR Systems, Industrial & Engineering Chemistry Research, 49 (2010) 6332-6341.

[7] S.S.R. Putluru, L. Schill, A. Godiksen, R. Poreddy, S. Mossin, A.D. Jensen, R. Fehrmann, Promoted V_2O_5/TiO_2 catalysts for selective catalytic reduction of NO with NH_3 at low temperatures, Applied Catalysis B: Environmental, 183 (2016) 282-290.

[8] Q.-l. Chen, R.-t. Guo, Q.-s. Wang, W.-g. Pan, W.-h. Wang, N.-z. Yang, C.-z. Lu, S.-x. Wang, The catalytic performance of Mn/TiWOx catalyst for selective catalytic reduction of NOx with NH_3, Fuel, 181 (2016) 852-858.

[9] W. Sjoerd Kijlstra, M. Biervliet, E.K. Poels, A. Bliek, Deactivation by SO_2 of MnOx/Al_2O_3 catalysts used for the selective catalytic reduction of NO with NH_3 at low temperatures, Applied Catalysis B: Environmental, 16 (1998) 327-337.

[10] S.S.R. Putluru, L. Schill, A.D. Jensen, B. Siret, F. Tabaries, R. Fehrmann, Mn/TiO_2 and Mn–Fe/TiO_2 catalysts synthesized by deposition precipitation—promising for selective catalytic reduction of NO with NH_3 at low temperatures, Applied Catalysis B: Environmental, 165 (2015) 628-635.

[11] H. Zhao, X. Mu, C. Zheng, S. Liu, Y. Zhu, X. Gao, T. Wu, Structural defects in 2D MoS_2 nanosheets and their roles in the adsorption of airborne elemental mercury, Journal of Hazardous Materials, 366 (2019) 240-249.

[12] W.S. Kijlstra, D.S. Brands, E.K. Poels, A. Bliek, Mechanism of the Selective Catalytic Reduction of NO by NH_3 over MnOx/Al_2O_3 I. Adsorption and Desorption of the Single Reaction Journal of Catalysis, 171 (1997) 208-218.

[13] Y.J. Kim, H.J. Kwon, I.-S. Nam, J.W. Choung, J.K. Kil, H.-J. Kim, M.-S. Cha, G.K. Yeo, High deNOx performance of Mn/TiO_2 catalyst by NH_3, Catalysis Today, 151 (2010) 244-250.

[14] F. Kapteijn, L. Singoredjo, A. Andreini, J.A. Moulijn, Activity and selectivity of pure manganese oxides in the selective catalytic reduction of nitric oxide with ammonia, Applied Catalysis B: Environmental, 3 (1994) 173-189.

[15] J. Zhu, A. Thomas, Perovskite-type mixed oxides as catalytic material for NO removal, Applied Catalysis B: Environmental, 92 (2009) 225-233.

[16] C. Fang, D. Zhang, S. Cai, L. Zhang, L. Huang, H. Li, P. Maitarad, L. Shi, R. Gao, J. Zhang, Low-temperature selective catalytic reduction of NO with NH_3 over nanoflaky MnOx on carbon nanotubes in situ prepared via a chemical bath deposition route, Nanoscale, 5 (2013) 9199-9207.

[17] L. Yan, Y. Liu, K. Zha, H. Li, L. Shi, D. Zhang, Scale–Activity Relationship of MnOx-FeOy Nanocage Catalysts Derived from Prussian Blue Analogues for Low-Temperature NO Reduction: Experimental and DFT Studies, ACS Applied Materials & Interfaces, 9 (2017) 2581-2593.

[18] K. Zha, L. Kang, C. Feng, L. Han, H. Li, T. Yan, P. Maitarad, L. Shi, D. Zhang, Improved NOx reduction in the presence of alkali metals by using hollandite Mn–Ti oxide promoted Cu-SAPO-34 catalysts, Environmental Science: Nano, 5 (2018) 1408-1419.

[19] C. Li, X. Tang, H. Yi, L. Wang, X. Cui, C. Chu, J. Li, R. Zhang, Q. Yu, Rational design of template-free MnOx-CeO_2 hollow nanotube as de-NOx catalyst at low temperature, Applied Surface Science, 428 (2018) 924-932.

[20] X. Hu, L. Huang, J. Zhang, H. Li, K. Zha, L. Shi, D. Zhang, Facile and template-free fabrication of mesoporous 3D nanosphere-like $Mn_xCo_{3-x}O_4$ as highly effective catalysts for low temperature SCR of NOx with NH_3, Journal of Materials Chemistry A, 6 (2018) 2952-2963.
[21] K. Zha, S. Cai, H. Hu, H. Li, T. Yan, L. Shi, D. Zhang, In Situ DRIFTs Investigation of Promotional Effects of Tungsten on MnOx-CeO_2/meso-TiO_2 Catalysts for NOx Reduction, The Journal of Physical Chemistry C, 121 (2017) 25243-25254.
[22] L. Huang, X. Hu, S. Yuan, H. Li, T. Yan, L. Shi, D. Zhang, Photocatalytic preparation of nanostructured MnO_2-(Co_3O_4)/TiO_2 hybrids: The formation mechanism and catalytic application in SCR deNOx reaction, Applied Catalysis B: Environmental, 203 (2017) 778-788.
[23] R. Jin, Y. Liu, Z. Wu, H. Wang, T. Gu, Low-temperature selective catalytic reduction of NO with NH_3 over Mn-Ce oxides supported on TiO_2 and Al_2O_3: a comparative study, Chemosphere, 78 (2010) 1160-1166.
[24] G. Qi, R.T. Yang, Low-temperature selective catalytic reduction of NO with NH_3 over iron and manganese oxides supported on titania, Applied Catalysis B: Environmental, 44 (2003) 217-225.
[25] N.-z. Yang, R.-t. Guo, W.-g. Pan, Q.-l. Chen, Q.-s. Wang, C.-z. Lu, The promotion effect of Sb on the Na resistance of Mn/TiO_2 catalyst for selective catalytic reduction of NO with NH_3, Fuel, 169 (2016) 87-92.
[26] L. Liu, C. Zheng, J. Wang, Y. Zhang, X. Gao, K. Cen, NO Adsorption and Oxidation on Mn Doped CeO_2 (111) Surfaces: A DFT+ U Study, Aerosol and Air Quality Research, 18 (2018) 1080-1088+ ap1081.
[27] H. Zhao, X. Mu, G. Yang, M. George, P. Cao, B. Fanady, S. Rong, X. Gao, T. Wu, Graphene-like MoS_2 containing adsorbents for Hg^0 capture at coal-fired power plants, Applied Energy, (2017).
[28] F. Cao, S. Su, J. Xiang, P. Wang, S. Hu, L. Sun, A. Zhang, The activity and mechanism study of Fe–Mn–Ce/γ-Al_2O_3 catalyst for low temperature selective catalytic reduction of NO with NH_3, Fuel, 139 (2015) 232-239.
[29] L. Chen, J. Li, M. Ge, DRIFT Study on Cerium− Tungsten/Titiania Catalyst for Selective Catalytic Reduction of NOx with NH_3, Environmental science & technology, 44 (2010) 9590-9596.
[30] S. Zhang, B. Zhang, B. Liu, S. Sun, A review of Mn-containing oxide catalysts for low temperature selective catalytic reduction of NOx with NH_3: reaction mechanism and catalyst deactivation, RSC Advances, 7 (2017) 26226-26242.
[31] H. Zhao, X. Luo, J. He, C. Peng, T. Wu, Recovery of elemental sulphur via selective catalytic reduction of SO_2 over sulphided CoMo/γ-Al_2O_3 catalysts, Fuel, 147 (2015) 67-75.
[32] H. Zhao, G. Yang, X. Gao, C. Pang, S.W. Kingman, T. Wu, Hg0 capture over CoMoS/γ-Al_2O_3 with MoS_2 nanosheets at low temperatures, Environmental Science & Technology, (2015).
[33] C. Zhou, X. Liu, C. Wu, Y. Wen, Y. Xue, R. Chen, Z. Zhang, B. Shan, H. Yin, W.G. Wang, NO oxidation catalysis on copper doped hexagonal phase $LaCoO_3$: a combined experimental and theoretical study, Physical Chemistry Chemical Physics, 16 (2014) 5106-5112.
[34] Q. Yan, S. Chen, C. Zhang, Q. Wang, B. Louis, Synthesis and catalytic performance of Cu1Mn0.5Ti0.5Ox mixed oxide as low-temperature NH3-SCR catalyst with enhanced SO2 resistance, Applied Catalysis B: Environmental, 238 (2018) 236-247.
[35] Z. Liu, J. Zhu, S. Zhang, L. Ma, S.I. Woo, Selective catalytic reduction of NOx by NH3 over MoO3-promoted CeO2/TiO2 catalyst, Catalysis Communications, 46 (2014) 90-93.
[36] B. Shen, X. Zhang, H. Ma, Y. Yao, T. Liu, A comparative study of Mn/CeO2, Mn/ZrO2 and Mn/Ce-ZrO2 for low temperature selective catalytic reduction of NO with NH3 in the presence of SO2 and H2O, Journal of Environmental Sciences, 25 (2013) 791-800.
[37] P. Gong, J. Xie, D. Fang, D. Han, F. He, F. Li, K. Qi, Effects of surface physicochemical properties on NH_3-SCR activity of MnO_2 catalysts with different crystal structures, Chinese Journal of Catalysis, 38 (2017) 1925-1934.
[38] J. Xiang, L. Wang, F. Cao, K. Qian, S. Su, S. Hu, Y. Wang, L. Liu, Adsorption properties of NO and NH_3 over MnOx based catalyst supported on γ-Al_2O_3, Chemical Engineering Journal, 302 (2016) 570-576.
[39] L. Cheng, Y. Men, J. Wang, H. Wang, W. An, Y. Wang, Z. Duan, J. Liu, Crystal facet-dependent reactivity of α-Mn_2O_3 microcrystalline catalyst for soot combustion, Applied Catalysis B: Environmental, 204 (2017) 374-384.
[40] H.-L. Koh, H.-K. Park, Characterization of MoO_3–V_2O_5/Al_2O_3 catalysts for selective catalytic reduction of NO by NH_3, Journal of Industrial and Engineering Chemistry, 19 (2013) 73-79.

[41] O.A. Bulavchenko, T.N. Afonasenko, P.G. Tsyrul'nikov, S.V. Tsybulya, Effect of heat treatment conditions on the structure and catalytic properties of $MnOx/Al_2O_3$ in the reaction of CO oxidation, Applied Catalysis A: General, 459 (2013) 73-80.
[42] K. Li, R. Wang, J. Chen, Hydrodeoxygenation of anisole over silica-supported Ni_2P, MoP, and NiMoP catalysts, Energy & Fuels, 25 (2011) 854-863.
[43] D. Fang, J. Xie, H. Hu, H. Yang, F. He, Z. Fu, Identification of MnOx species and Mn valence states in $MnOx/TiO_2$ catalysts for low temperature SCR, Chemical Engineering Journal, 271 (2015) 23-30.
[44] L. Ma, Y. Cheng, G. Cavataio, R.W. McCabe, L. Fu, J. Li, In situ DRIFTS and temperature-programmed technology study on NH_3-SCR of NOx over Cu-SSZ-13 and Cu-SAPO-34 catalysts, Applied Catalysis B: Environmental, 156-157 (2014) 428-437.
[45] W.S. Kijlstra, D.S. Brands, H.I. Smit, E.K. Poels, A. Bliek, Mechanism of the Selective Catalytic Reduction of NO with NH_3 over $MnOx/Al_2O_3$ II. Reactivity of Adorbed NH_3 and NO Complexes, Journal of Catalysis, 171 (1997) 219-230.
[46] Z. Liu, S. Zhang, J. Li, L. Ma, Promoting effect of MoO_3 on the NOx reduction by NH_3 over CeO_2/TiO_2 catalyst studied with in situ DRIFTS, Applied Catalysis B: Environmental, 144 (2014) 90-95.
[47] G. Marbán, T. Valdés-Solís, A.B. Fuertes, Mechanism of low-temperature selective catalytic reduction of NO with NH_3 over carbon-supported Mn_3O_4: Role of surface NH_3 species: SCR mechanism, Journal of Catalysis, 226 (2004) 138-155.
[48] G. Marban, T. Valdes-Solis, A.B. Fuertes, Mechanism of low temperature selective catalytic reduction of NO with NH_3 over carbon-supported Mn_3O_4 Active phase and role of surface NO species, Physical Chemistry Chemical Physics, 6 (2004) 453-464.